In Situ Wide- and Small-Angle X-ray Scattering Study of Melting Kinetics of Isotactic Poly(propylene)

ARTICLE *in* MACROMOLECULES · MAY 2003

Impact Factor: 5.8 · DOI: 10.1021/ma025987z

5 AUTHORS, INCLUDING:

Peggy Cebe
Tufts University
248 PUBLICATIONS **4,658** CITATIONS

SEE PROFILE

R. G. Alamo
Florida State University
153 PUBLICATIONS **3,515** CITATIONS

SEE PROFILE

In Situ Wide- and Small-Angle X-ray Scattering Study of Melting Kinetics of Isotactic Poly(propylene)

Patrick S. Dai,[†] Peggy Cebe,*[,†] Malcolm Capel,[‡,#] Rufina G. Alamo,[§] and Leo Mandelkern[⊥]

Physics and Astronomy Department, Tufts University, Medford, Massachusetts 02155; Biology Department, Brookhaven National Laboratory, Upton, New York 11973; Chemical Engineering Department, Florida Agricultural and Mechanical University and Florida State University, Tallahassee, Florida 32310; and Department of Chemistry and Biochemistry, Florida State University, Tallahassee, Florida 32306

Received December 19, 2002; Revised Manuscript Received March 20, 2003

ABSTRACT: We describe a comparative study of long time isothermal melting kinetics of Ziegler−Natta catalyzed, and metallocene catalyzed, isotactic poly(propylenes). The role of the transverse lamellae in stabilizing the crystalline structures against melting is presented in light of the different molecular chain architecture and lamellar structure of these poly(propylenes). Both poly(propylenes) were first isothermally crystallized at 152 °C. Real time in-situ wide- and small-angle X-ray scattering (WAXS and SAXS) were used to study isothermal melting kinetics in a temperature region between melting of transverse and dominant (radial) lamellae, i.e., when most transverse lamellae are molten. Changes in WAXS crystalline peak height, SAXS invariant, and Bragg peak height with time all confirm that Ziegler−Natta iPP had slower melting kinetics than metallocene iPP. Melting kinetics is, apparently, unique to poly(propylene) as a consequence of a favorable nearly orthogonal epitaxial crystallization. What is observed is the instability of the dominant thicker lamellae due to the removal of the epitaxy. Both Ziegler−Natta and metallocene catalyzed polymers show a prolonged, gradual decay of crystallinity with time. Hence, melting kinetics is a general phenomenon observed in poly(propylenes) that crystallize preferentially in the alpha (monoclinic) modification. The crystallization conditions under which these iPPs exhibit melting kinetics are when crystallization occurs at relatively low undercooling, when the crystallites are not subject to reorganization.

Introduction

Isotactic poly(propylene) of sufficient structural regularity crystallizes in the monoclinic or alpha modification and exhibits a unique lamellar branching via a process of homoepitaxy.[1−5] This specific lamellar branching was studied by Lotz and Wittmann[6] on the basis of geometrical and structural models proposed by Padden and Keith[1,5] and Binsbergen and De Lange.[2] Profuse lamellar branching takes place by a nearly orthogonal growth on the lateral (010) faces of parent lamellae due to the near identity of the *a* and *c* axes of the monoclinic unit cell and a favorable interdigitation of methyl groups in the facing planes. At moderate undercooling, radial and transverse lamellae grow simultaneously during the early stages of the crystallization.[7,8] The homoepitaxy influences morphological features and may also affect thermodynamic properties of poly(propylenes). At the level of atomic force or electron microscopy, different arrays of crosshatched lamellae are observed depending on undercooling.[9−12] While crystallization temperatures below ∼140 °C lead to a mesh type of orthogonally grown lamellae with small differences in their thicknesses, the spherulites formed at temperatures above ∼145 °C show two populations of lamellae. Radially grown lamellae are thicker than the epitaxially grown "cross-hatched" lamellae.[9,10,13]

The fusion of isothermally crystallized isotactic poly(propylene), iPP, results in broad or double melting endotherms.[9] It has been shown that the two endotherms are a result of successive melting of the transverse and radial lamellae.[14] It was demonstrated in a recent communication that, after the melting of transverse lamella takes place, there is a significant kinetics involved in the fusion of the radial, thicker lamellae.[16] For example, it takes a relatively long time for melting to occur isothermally at a temperature just above the low-temperature endotherm as compared to a temperature just below the high-temperature one. These observations were made by following the decrease of the heat of fusion, measured by DSC, with time of iPPs annealed at temperatures at which most transverse lamellae are molten, i.e., between the two endotherms. The studies involved both Ziegler−Natta (ZN) and metallocene (M) catalyzed iPPs. It was concluded that thicker radial lamellae become unstable due to the melting of transverse lamellae. The melting kinetics makes difficult the determination of the true melting temperature, the lowest annealing temperature at which the sample would melt after an infinite annealing time. It also makes it difficult to employ any of the standard extrapolation procedures that are conventionally used in order to obtain the equilibrium melting temperature of isotactic poly(propylene).[17] This phenomenon can well be a major reason that such a range in values has been reported for the equilibrium melting temperature of isotactic poly(propylene).[18−21]

[†] Tufts University.
[‡] Brookhaven National Laboratory.
[§] Florida Agricultural and Mechanical University and Florida State University.
[⊥] Florida State University.
[#] Present address: Advanced Photon Source, Argonne National Laboratory, Argonne, IL.
* Corresponding author: e-mail peggy.cebe@tufts.edu.

10.1021/ma025987z CCC: $25.00
Published on Web 05/08/2003

Table 1. Structural Characteristics of Isotactic Polypropylenes

sample	catalyst type	M_w (g/mol)	M_w/M_n	stereo defects (mol %)	regio defects (mol %)	isotacticity (mmmm)
ZN	Ziegler−Natta	312 300	4.5	1.02	0	0.93
M	metallocene	349 000	2.5	0.09	0.35	0.99

Table 2. Sample Preparation and Thermal Properties of Isotactic Poly(propylenes)

catalyst type	crystallization 152 °C for 10 days	T_{m1}[a] (°C)	T_{m2}[b] (°C)	degree of crystallinity[c] (%)
Ziegler−Natta ZN-v	in a vacuum	171.7	180.0	58
metallocene M-v	in a vacuum	174.3	178.6	62
Ziegler−Natta ZN-n	in nitrogen	172.4	179.7	59
metallocene M-n	in nitrogen	175.7	179.7	58

[a] Melting of transverse lamella. [b] Melting of dominant lamella. [c] Degree of crystallinity from enthalpy of fusion determined from the total area of the upper and lower melting endotherms.

In the present work real-time, simultaneous wide- and small-angle X-ray scattering (WAXS and SAXS) were used to study the melting kinetics of ZN and M poly(propylenes) that had been crystallized at a high temperature, for a long time. After crystallization the samples were heated to an isothermal annealing, or holding, temperature located between the two melting endotherms. Structural parameters such as the scattering invariant, Bragg spacings, long period, and lamellar thickness are measured as functions of time in order to extract the evolution of the lamellar structure during isothermal melting.

Experimental Section

Sample Characterization. Two isotactic poly(propylene) samples were used in this study. One is a commercial iPP synthesized with a Ziegler−Natta type catalyst and is designated as ZN. The other was synthesized with a metallocene type catalyst and is designated as M. The main structural characteristics of the polymers are listed in Table 1.

Both polymers have similar weight-average molecular weights. However, the ZN polymer has much broader molecular weight distribution, a higher content of stereo defects, and no regio defects. The molecular weight distributions were obtained by standard GPC methods.[22] The concentrations of stereo and regio defects were determined by high-resolution ^{13}C NMR. The concentrations of regio defects were calculated from the appropriate NMR peaks.[23−25] The stereo defects were determined from half of the fraction of mmmr pentads.[26]

Compression-molded films were placed in either vacuum- or nitrogen-sealed glass tubes. After the samples were melted at 200 °C for 10 min, the tubes were rapidly transferred to a thermostated oil bath preset at 152 ± 0.1 °C. After a 10 day isothermal crystallization period the tubes were quenched by rapidly transferring from the oil bath to ice water. The crystallization at 152 °C was complete, and the cooling through quenching to ice water did not introduce any significant amount of new crystals. This was demonstrated by the insignificant quenching peak observed after a subsequent melting of the isothermally crystallized samples (see Figure 1). Both sets of samples, crystallized in a vacuum (v) or under nitrogen (n), were studied and are labeled ZN-v, ZN-n, M-v, and M-n.

Differential scanning calorimetry was performed on a Perkin-Elmer DSC-7 calibrated with indium. In all the DSC experiments, the heating rate was 10 °C/min and sample size was about 3 mg. The degrees of crystallinity were calculated from the observed heat of fusion using $\Delta H_u = 2100$ cal/mol as the heat of fusion of the pure monoclinic poly(propylene).[27]

Atomic Force Microscopy. For AFM imaging a film of each iPP was sandwiched between two glass coverslips and placed in a vacuum-sealed glass tube. Crystallization was carried out following identical procedures as for the samples used in simultaneous WAXS/SAXS experiments. The lamellar morphology of the ZNiPP was imaged using a Dimension III instrument from Digital Instruments, Inc. The MiPP sample was imaged using a JEOL 4210 instrument. An Olympus brand silicone tip oscillating slightly below its resonance frequency (~300 kHz) was used to scan the surface by a noncontact mode. The output images were collected in the form of topography and phase images simultaneously.

Thermal Treatment for Isothermal Melting. The procedure established to follow the isothermal melting for all four samples was as follows. The samples were initially rapidly heated to 130 °C and held there for 1 min. They were then heated from 130 to 170 °C at 5 °C/min. This stage, called the initial, fast heating stage, brings the temperature to the peak of the lower melting endotherm. A lower heating rate was used subsequently in approaching the annealing temperatures to prevent overheating from possible thermal lags. The heating rate was then reduced to 0.3 °C/min as the sample was heated from 170 °C to the predetermined temperature, T_i, to study isothermal melting. The temperature T_i was set at 174.5 °C for the two ZN samples and 174.0 for the M samples. This stage, called the second, slow heating stage, raises the temperature to a point about midway between the upper and lower melting endotherms. After the temperature reaches T_i, the sample is held at that temperature for 140 min for the ZN polymers and 100 min for the M polymer.

X-ray Scattering. Real-time small-angle X-ray scattering (SAXS) and wide-angle X-ray scattering (WAXS) experiments were performed at beamline X12B of the National Synchrotron Light Source at Brookhaven National Laboratory (BNL). Monochromatic X-radiation with a wavelength $\lambda = 1.6$ Å was used. The sample was located inside a Mettler FP80 hot stage between two layers of Kapton tape. Both SAXS and WAXS data were taken continuously during the experiment, and each scan was of 60 s duration. The detector for SAXS was a BNL custom-built two-dimensional, histogramming gas-filled wire detector[28,29] with 512 × 512 channels.

The SAXS data were collected and analyzed by methods described earlier.[28,29] Several quantities were calculated from SAXS data. The scattering invariant, Q, is found from ref 31:

$$Q = \int_0^\infty I(q) q^2 \, dq \tag{1}$$

For a two-phase system[31,32]

$$Q \sim \chi_c(1 - \chi_c)(\Delta\rho)^2 \tag{2}$$

where χ_c and $(1 - \chi_c)$ are respectively the volume fractions of the crystalline and amorphous phases, and $\Delta\rho = \rho_c - \rho_a$ is the density difference measured in electrons per unit volume. $\Delta\rho$ is also called the "scattering contrast". If the entire sample volume is filled with lamellar stacks, the total crystalline fraction, χ_c, will correspond to the fraction of crystallinity determined from DSC (placed on a volume basis). We can also consider that during melting or crystallization a fraction χ_s of the polymer is transformed into spherulites while the rest is amorphous and that the spherulites are filled with lamellae stacks separated by amorphous layers. If the fractional content of crystalline lamellae within a stack is χ_{cl}, then the total crystallinity is related to the lamellar stack crystallinity by $\chi_c = \chi_{cl}\chi_s$. In this case the invariant has the following form:

$$Q \sim \chi_s\chi_{cl}(1 - \chi_{cl})(\Delta\rho)^2 \tag{3}$$

When thick, long radial lamellae and thin, short transverse lamellae coexist within the spherulites, we may consider the invariant to result from the sum of the scattering from stacks of radial lamella (R) and the scattering from stacks of transverse lamellae (T). Then, $\chi_{cl} = \chi_{cl}^R + \chi_{cl}^T$, and on the

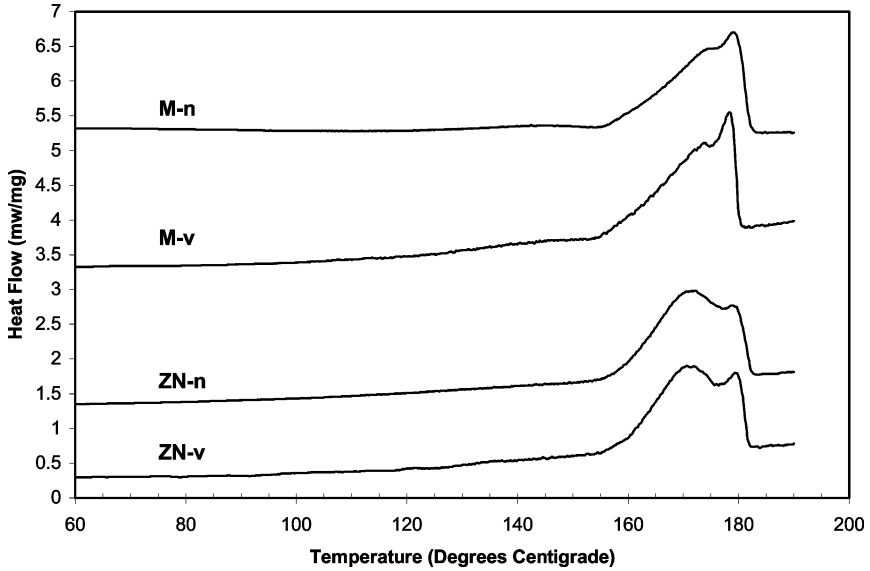

Figure 1. Differential scanning calorimetry scans at 10 °C/min for isotactic polypropylene samples that had been crystallized at 152 °C for 10 days (in a vacuum, v; in nitrogen, n). Ziegler−Natta samples, ZN-v and ZN-n, and metallocene samples M-v and M-n.

assumption that the spherulite volume is unity, we can write Q as

$$Q \sim \chi_{cl}{}^{R}\chi_s(1-\chi_{cl}{}^{R})(\rho_c-\rho_i)^2 + \chi_{cl}{}^{T}\chi_s(1-\chi_{cl}{}^{T})(\rho_c-\rho_a)^2 \quad (4)$$

The radial lamellae scatter with a contrast factor that reflects the difference between the crystal phase and the intervening phase, which is filled with transverse lamellar stacks. The transverse lamellae scatter with a contrast factor arising from the difference of the crystal density and the completely amorphous phase density. When transverse lamellae melt, the effect is that the phase intervening between the radial lamellae has $\rho_i = \rho_a$.

Lamellar thickness was calculated from the one-dimensional electron density correlation function.[32] Simple application of Bragg's law was used to find the long spacing of the major (more intense) and the minor (less intense) scattering peaks of the Lorentz corrected intensity.

The WAXS data were collected with a Braun 7 cm one-dimensional position-sensitive gas-filled wire detector. The detector operated at 3 kV, with argon/methane (90/10) gas flowing at 1 mL/min. The d spacings were calibrated by reference to the scattering peak (200) of NaCl powder (a = 5.63 Å) and scattering peaks (111) and (200) of KBr powder (a = 6.59 Å). The 2θ angular range covered by the wide-angle detector was 9.4°−41.2°. Scans were collected for 60 s simultaneously with the SAXS scans. All WAXS data were first corrected for background. Finally, for calculation of relative WAXS peak heights, the amorphous scattering curve from the completely melted state was scaled and subtracted from the data.

Only the α crystal polymorph was observed in this study. The changes in the crystalline peak heights were used as indicators of the melting kinetics. The time dependence of the crystal height, $H_c(t)$, is written in terms of the amorphous height, H_a, and total curve height, H_T, as

$$H_c(t) = H_T(t) - H_a(t) \quad (5)$$

H_c is normalized so that $H_c(t=0) = 1$. In the melt state, $H_T(t_{melt}) = H_a(t_{melt})$.

Results and Discussion

Thermograms of the four samples studied are given in Figure 1. All four are qualitatively similar to one another. Typically, each shows two melting endotherms. Detailed studies have identified the origin of the two peaks.[9] Most branched thinner tangential lamellae melt cooperatively in the temperature region represented by the low-temperature endotherm, T_{m1}, while melting of thicker radial lamellae is represented by the higher temperature endotherm, T_{m2}. Their respective values are given in Table 2. The difference in the two peaks ranges from 4 to 9 °C. Also given in the table is the degree of crystallinity calculated from the enthalpy of fusion. Although the metallocene type has an average concentration of defects about half that of the ZN, there are no significant differences in either the higher melting peaks or degrees of crystallinity between the two types of polypropylenes as seen in Table 2. This is a consequence of the differences in distribution of defects in both poly(propylenes). It is known that the defects in the metallocene sample are randomly distributed intramolecularly, and the interchain composition is uniform.[33] The interchain defect composition in the ZN type is broad and presents a blocky intrachain distribution.[33,34] There is a fraction of highly defected molecules in the ZN type that likely do not participate in the crystallization. Thus, the effective average concentration of defects for crystallization of the ZN sample is lower than the polymer overall concentration, leading to melting temperatures higher than those expected for a polymer with uniform concentration and randomly distributed defects.

The lamellar morphology as discerned by AFM is illustrated in Figure 2a,b for the ZN and M polymers that were crystallized at 152 °C. Profuse crosshatching is observed in both poly(propylenes). However, the difference in tacticity distribution between the ZN and M types imparts some important differences between the two lamellar structures. The crosshatched lamellae in the ZN sample show high contrast. Long radial lamellae and thinner crosshatched ones are observed. In contrast, the M polymer forms thinner segmented lamellae with less contrasted crosshatching. The lamellae in the M polymer appear twisted and more disorganized. These observations indicate that the M polymer, with a uniform interchain defect distribution, acts more like a random type copolymer. On the other

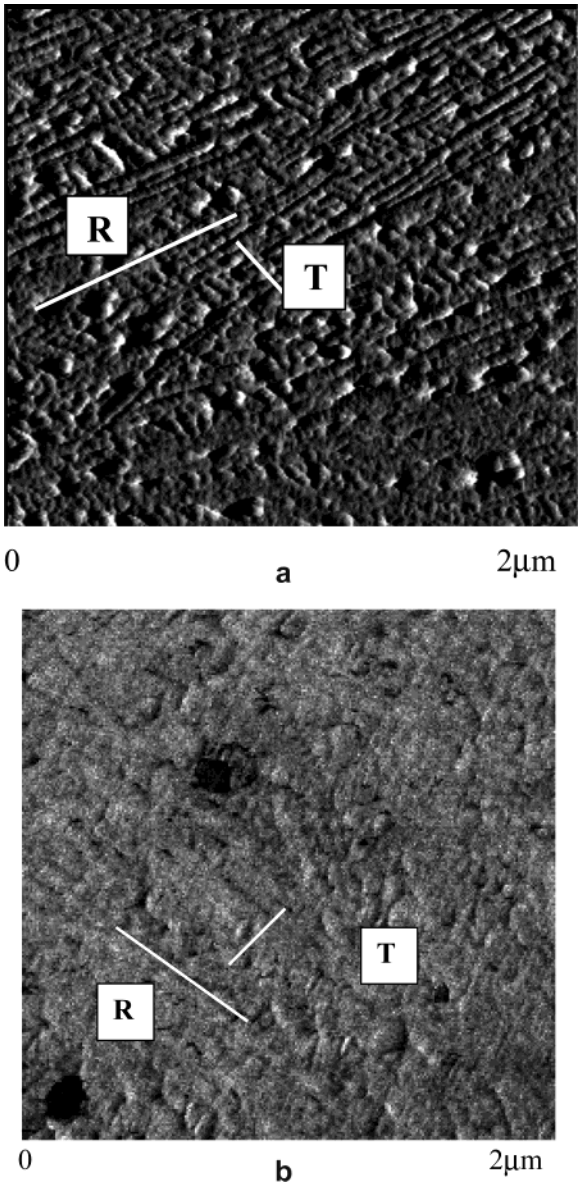

Figure 2. Atomic force microscopy phase images showing details of lamellar structure in iPP crystallized at 152 °C (full scale width is 2 μm): (a, top) Ziegler−Natta iPP; (b, bottom) metallocene iPP. The orientations of most radial and most transverse lamellae are indicated by lines.

hand, in the unfractionated ZN polymer, the very low defected higher molecular weight chains appear to dominate or direct the crystallization leading to more contrast between longer and shorter crosshatched lamellae. The structural differences in lamellae perfection, and in the amount and nature of the transverse and radial lamellae, provide the basis for the observed variation in melting kinetics between the ZN and M samples.

The metallocene samples crystallized either in a vacuum or nitrogen showed no differences in distribution of scattered X-ray intensity, or the structural parameters derived from intensity, in either wide- or small-angle X-ray studies. Ziegler−Natta samples crystallized in either vacuum or nitrogen did show some differences in their wide- and small-angle X-ray scattering behavior. This in turn was reflected in the kinetics of melting. The vacuum-crystallized polymer never completely melted during the isothermal holding period.

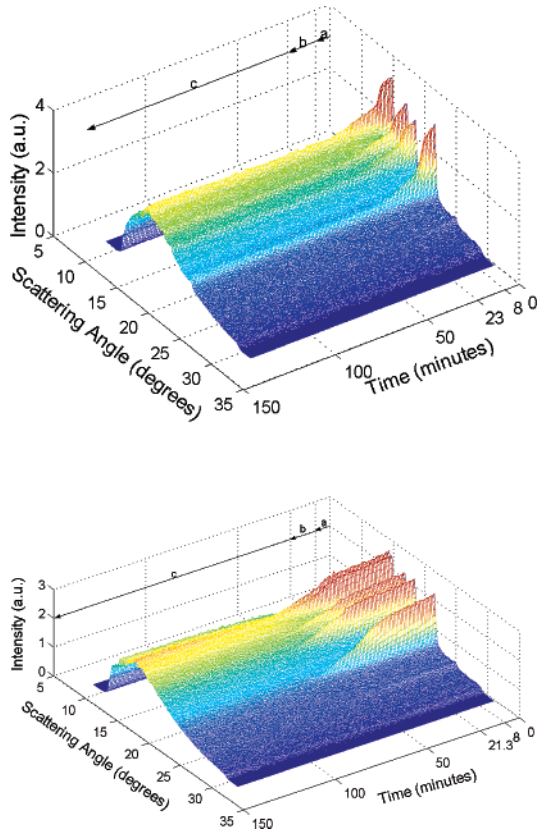

Figure 3. Three-dimensional plot of wide-angle X-ray scattering intensity vs scattering angle vs time, during heating at 5 °C/min from 130 to 170 °C (first 8 min marked by arrow a), then heating at 0.3 °C/min from 170 °C to T_i, the isothermal holding temperature (for ZN-v, next 15 min; for M-n, next 13.3 min, marked by arrow b), followed by isothermal holding for the remaining time shown (marked by arrow c). (a) Upper plot: Ziegler−Natta iPP sample ZN-v, $T_i = 174.5$ °C. (b) Lower plot: metallocene iPP sample M-n, $T_i = 174$ °C (peak positions shown for X-ray wavelength, $\lambda = 0.160$ nm.)

Parts a and b of Figure 3 give three-dimensional plots of the WAXS scattering intensity vs scattering angle vs time for ZN-v and M-n polymers, respectively, during heating and isothermal holding at T_i.

In the figure, the first 8 min represents the heating of the samples at 5 °C/min from 130 to 170 °C that includes the peak of the low melting endotherm. This region is marked by arrow a. Both samples display only a slight decrease in WAXS intensity during this portion of the heating, as the temperature increases through the low-temperature endotherm. The next 15 min for the ZN-v sample (Figure 3a) or 13.3 min for the M-n sample (Figure 3b) represents the second-stage heating, at a slower heating rate of 0.3 °C/min, from 170 °C up to the isothermal holding temperature between the two endotherms. This region is marked by arrow b. For the ZN-v polymer the isothermal holding temperature is 174.5 °C, while the M polymer is slightly lower, at 174.0 °C. These temperatures were chosen on the basis of previous isothermal melting data obtained by DSC, where it was found that after crystallization at 152 °C complete melting took place at annealing temperatures between 0.5 and 1 °C higher for the ZN sample than for a metallocene one.[16] During the second stage heating, the temperature increases from the lower endotherm peak up to a point between the two endotherms.

The WAXS intensity of the ZN-v polymer drops significantly during the second state of slow heating.

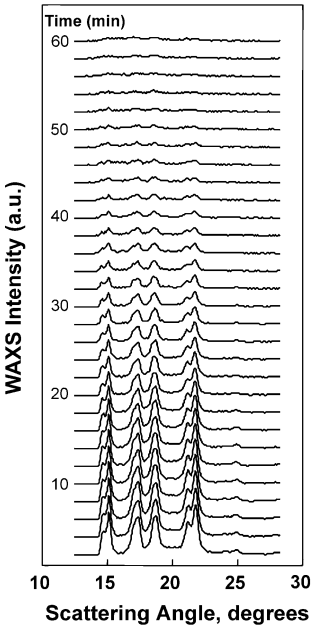

Figure 4. WAXS intensity vs scattering angle for M-v during isothermal holding at 174 °C for 60 min, at 2 min intervals. Complete melting is taking place at ~52−54 min. Diffractograms are shifted vertically for clarity (peak positions shown for X-ray wavelength, $\lambda = 0.160$ nm).

Once the isothermal holding temperature has been reached (marked by arrow c), the intensity drops more slowly. After annealing at 174.5 °C for 120 min, DSC experiments indicated complete melting. However, remnants of crystalline diffraction peaks are still observed, suggesting that a small fraction of the thickest ZN lamellae remain unmelted while their heat of fusion is broad and too small to be detected in the DSC experiment.

In contrast, the metallocene sample, M-n, in Figure 3b, shows a very gradual reduction of intensity for the first 40 min. This includes both the heating stages and a portion of isothermal period. After about 70 min (or, after a total of 50 min of isothermal holding at 174 °C) all of the crystal peaks have disappeared. The metallocene sample crystallized in a vacuum behaved in a similar manner. Upon completion of the isothermal holding time the samples were reheated to 220 °C, and the WAXS scans were recorded. There were no crystalline diffraction peaks remaining in any of the samples, and the amorphous halo strengthened in intensity as temperature increased.

The results in Figure 3a,b indicate that there is a definite kinetics to the fusion process when the sample is held at a temperature between the endotherms confirming previous DSC results.[16] This conclusion can be seen more clearly when the WAXS intensities at the holding temperature are plotted for different times. As an example, the data for M-v are given in Figure 4. Here the WAXS intensity (after subtraction of the amorphous halo) at 174 °C is plotted at 2 min intervals and displaced in the ordinate axis for clarity. It is clear from this figure that the discrete Bragg reflections can be observed up to about 50−54 min. Thus, this sample does in fact melt at the holding temperature of 174 °C.

Further information with respect to the isothermal melting kinetics can be obtained by focusing attention on a specific Bragg spacing. Figure 5 illustrates the change in the relative WAXS peak height with time for the strong (130) reflection located at $2\theta \sim 18.54°$ ($\lambda =$ 0.16 nm) for the ZN-n (filled circles), ZN-v (plus signs), and M-v (open circles) polymer crystallized in a vacuum. (M-n has behavior identical to M-v, and it is not shown.)

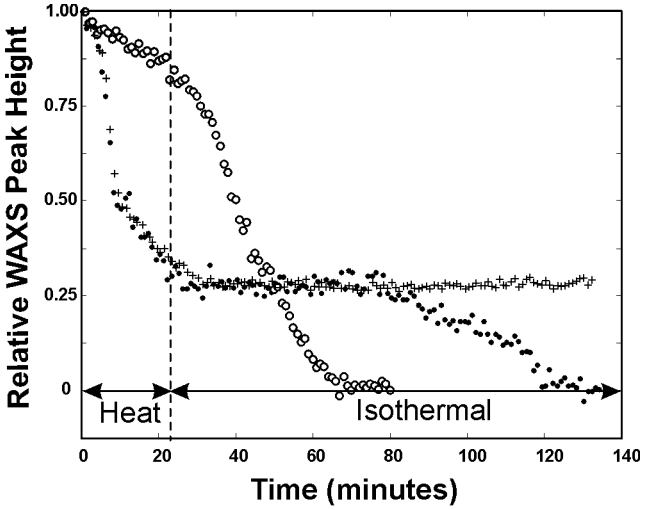

Figure 5. Relative WAXS peak height vs time, determined from the height of the reflection at scattering angle, 2θ of ~18.54° (for X-ray wavelength 0.160 nm), having Miller indices (130). Peak intensity is scaled from unity at the start of the experiment to zero when no crystalline reflections could be observed. ZN-n (filled circles); ZN-v (plus signs); M-v (open circles).

The curves show the decrease of the intensity of this reflection with time. Although only the time dependence of one peak is displayed, all of the crystalline peaks showed exactly the same trend. Here all the data are in the 1 min per point resolution, and the dashed line in the figure represents the beginning of the isothermal period. The peak height decrease for the M polymer is slow for the first 30 min and then continues more rapidly until the crystal peak disappears at about 70 min. The decrease of crystallinity during the heating stage of the ZN samples is very rapid and then progresses slowly up to about 80 min. The ZN-v sample shows insignificant melting for longer times up to 140 min while the sample prepared in nitrogen showed a progressive decrease of crystallinity up to complete melting at ~120 min. Hence, it seems that in a vacuum the ZN sample developed thicker, more stable lamellae requiring either much longer annealing times or higher annealing temperatures for complete melting. Interestingly, as seen in Figure 5, the disappearance of crystallinity with time in both types of poly(propylenes) suggests that isothermal melting is taking place in three stages: (1) An initial slow decay of crystallinity where it is postulated that a critical number of melting nuclei develop due to the disappearance of transverse lamellae. (2) A rapid cooperative stage follows with crystallinity decreasing rapidly. This stage probes the instability of dominant lamellae from the removal of the epitaxy. (3) A last stage where a few thicker, more stable crystallites slowly melt.

The availability of time-resolved in situ WAXS data during isothermal melting allows us to see details of the melting isotherm as seen in Figure 5. On the other hand, only the second stage of rapid decrease of crystallinity was obtained by discontinuous DSC experiments.[16] It is important to notice in Figure 5 that very long holding times at this temperature are required in order to see the melting, which could not be detected if shorter times were used.

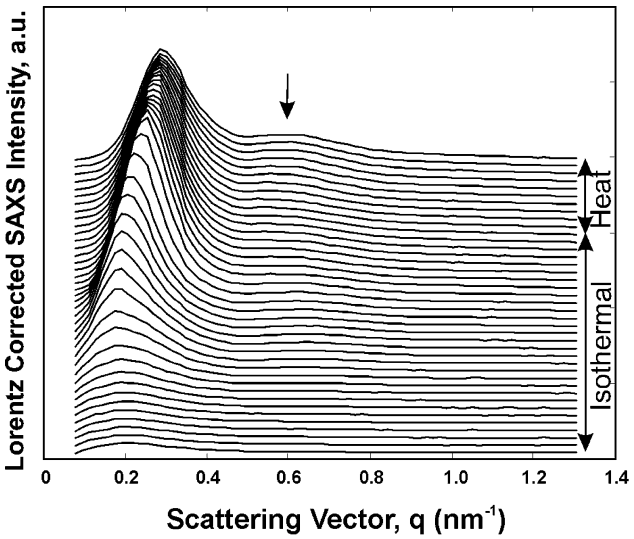

Figure 6. Composite plot of Lorentz-corrected SAXS intensity vs scattering vector, q, for metallocene iPP sample M-n. The scans begin with two-stage heating followed by isothermal holding at temperature T_i = 174 °C. The arrow marks the location of the secondary Bragg peak. Curves are shifted vertically for clarity.

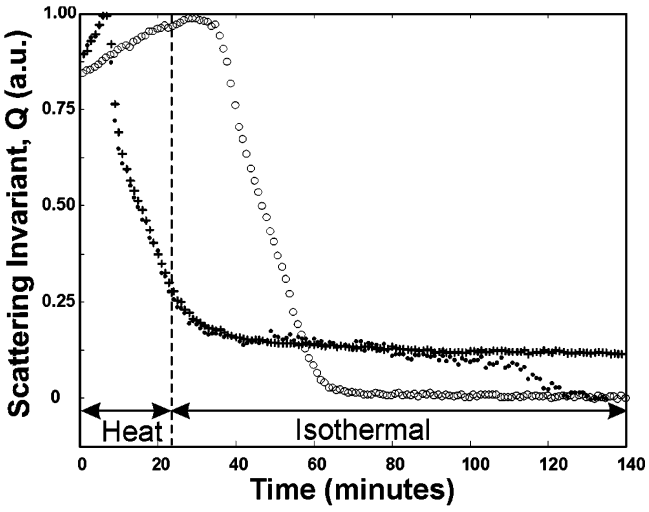

Figure 7. SAXS scattering invariant, Q, vs time, determined from the area under the Lorentz-corrected intensity. Ziegler−Natta iPP sample ZN-v, plus signs; Ziegler−Natta iPP sample ZN-n, solid circles; metallocene iPP sample M-n, open circles. The start of the isothermal period differs by 1.66 min for the two data sets, M-n and the ZN iPPs. Times correspond to the treatments described in the caption of Figure 3.

The SAXS patterns show similar effects with respect to isothermal melting. As an example, Figure 6 is a composite plot of the Lorentz-corrected SAXS intensity, $I(q)q^2$, vs scattering vector, q, during heating and isothermal holding at 174 °C for the M-n sample. The time sequence is from top to bottom, and the heating and isothermal holding periods are marked. Each scan in Figure 6 represents 1 min of data collection. The successive scans are separated by a 2 min time interval for clarity in the presentation. The scattering pattern of the initial M-n has two peaks: a major peak at $q \simeq 0.3$ nm^{-1} and a second smaller peak at $q \simeq 0.6$ nm^{-1}. The latter peak is marked with an arrow in the figure. All four samples exhibited the two SAXS maxima. The melt scans were never completely flat. They showed a slight bump due to uncompensated background, which persisted even when the samples were reheated to 220 °C. The melt scan was subtracted before any structural parameters were calculated. It is also quite clear from this figure that with time the two maxima disappear. This is indicative that melting has taken place isothermally and confirms the WAXS results.

Figure 7 gives the scattering invariant Q calculated from the Lorentz-corrected intensity according to eq 1. The trends between the invariant and the WAXS peak heights of Figure 5 are also similar. There is a minor difference between the two during the initial fast heating period. In this region, 130−170 °C, the invariant increases due to thermal expansion. The invariant decreases during the slow heating from 170 to 174 °C as a consequence of melting of transverse lamellae. This melting overcomes any thermal expansion of lamellar stacks in ZN samples. A slower decrease of the invariant is further seen in the isothermal period. For the vacuum-treated ZN sample, Q remains significantly above zero during the annealing time studied, in agreement with the results from WAXS. A fraction of the thickest crystallites remain unmelted at this time. Independent DSC studies have shown that complete melting of this sample would take between 5 and 6 h. The invariant for the ZN-n sample begins a slow decrease at 75 min and then a more rapid one following a similar type of sigmoidal behavior as observed in the WAXS data.

The invariant for the metallocene polymers also follows the trend of the WAXS data. After the period of thermal expansion, a sigmoidal rapid decrease is observed and Q decreases to zero. The first stage of the isotherm is considerably shorter in the metallocene polymers despite the lower T_i. This suggests a faster nucleation, which, in analogy to the crystallization process, may control the overall rate of melting. As a consequence, metallocene iPPs show faster melting kinetics than ZN iPPs as indicated by Figures 5 and 7.

The scattering invariant for the metallocene polymers rises dramatically, although WAXS peak height decreases, indicating that major melting is occurring. As a large fraction of transverse lamellae melt during the heating period, the remaining thicker lamellae scatter with improved contrast. By considering eq 4, we see that, during melting of transverse lamellae, the terms in the sum superscripted with T diminish to zero. This reflects the reduction through melting of the volume fraction of thinner crosshatched stacks and of the crystallinity in these stacks. Once the crosshatched lamellae melt, the intervening phase separating radial or dominant lamellae has improved scattering contrast. The first terms in the sum relating to dominant lamellae now are multiplied by a scattering contrast factor in which ρ_i is now replaced by ρ_a.

The scattering invariant shown in Figure 7 reflects the *integrated* area of both the major and minor SAXS scattering peaks. To examine the behavior of the individual peaks, each of their peak heights, taken as a measure of the relative scattering strength, is plotted in parts a and b of Figure 8 for ZN-n and M-n samples, respectively. The intensity of the minor peak for ZN-n basically disappears before the beginning of the isothermal period. Most of the intensity loss occurs during the initial stage fast heating. The major peak, on the other hand, strengthens during the first stage of fast heating. It then decreases rapidly during the slow heating second stage and the start of the isothermal period. Figure 8b gives the peak heights for the metallocene polymer on

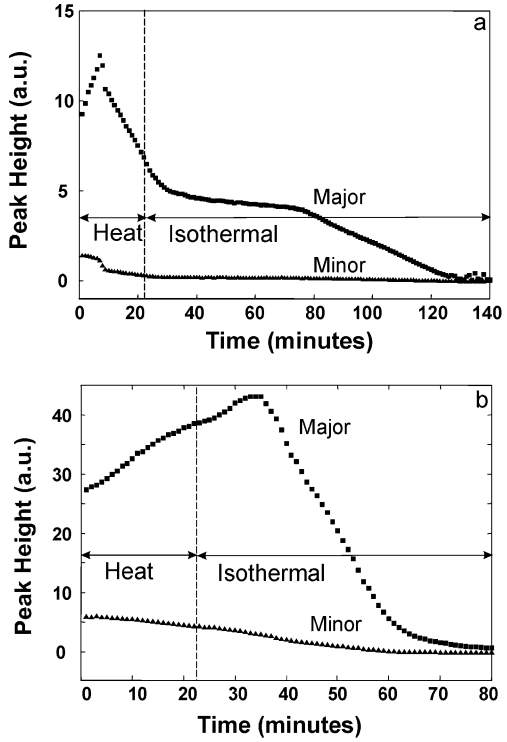

Figure 8. Relative peak heights of the major and minor Bragg reflections in the SAXS scans vs time: (a) Ziegler−Natta iPP sample ZN-n; (b) metallocene iPP sample M-n.

a shortened time scale. The scale reflects the more rapid melting kinetics in this polymer.

The intensity of the minor peak decreases slowly and continuously throughout the time period of heating and isothermal holding. The major peak increases during heating and the isothermal period and then decreases steadily. The different temperature dependence of the major and minor peaks confirms that they are not simply multiple orders of scattering from the same structure.

Parts a and b of Figure 9 present long spacing corresponding to the major and minor scattering peaks, respectively. The solid symbols refer to ZN-n sample while the open ones refer to the M-n polymer. Long periods of the initial samples before heating are 23 nm for the ZN sample and 21.7 nm for the metallocene, and a similar difference is reflected from the minor peaks (Figure 9b). Thus, there is a difference in the periodicity of the initial lamellar stacks of the ZN and M poly(propylenes) and also a different evolution of the lamellar structure during nonisothermal and, especially, during the isothermal melting regions. The long spacing increases sharply during the fast heating stages of the ZN polymer, but only a small increase is observed in for the M polymer in this stage. It remains constant for the ZN during most of the isothermal stage up to melting but increases continuously for the M due to fast melting and only remains invariant for the last 20 min of the isothermal stage, before complete melting.

Despite the higher noise level, some trends are also observed in the long spacing associated with the minor scattering peaks shown in Figure 9b. Although rather small compared with the major scattering peaks, in both polypropylenes the minor peak diminishes in intensity but persists throughout most of the isothermal holding period. These peaks may be associated with long-range order of lamellae stacks in the center of the spherulites

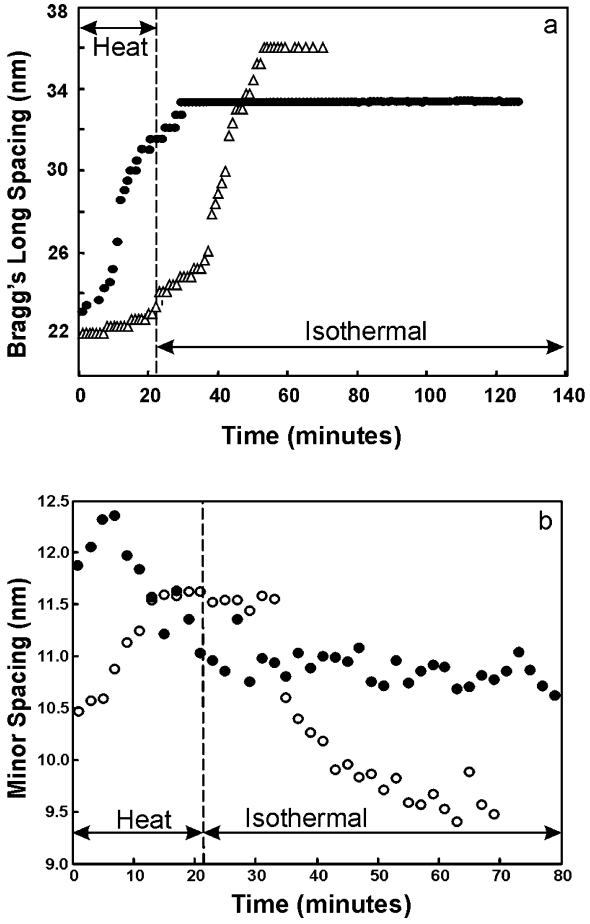

Figure 9. (a) Long period vs time and (b) minor peak spacing vs time, both determined from Bragg's law. Ziegler−Natta iPP sample ZN-n, solid symbols; metallocene iPP sample M-n, open symbols. The start of the isothermal period differs by 1.66 min for the two data sets, M-n and ZN-n. Times correspond to treatments described in the caption of Figure 3.

where the interlamellar region is significantly reduced compared with other peripheral regions of the spherulites. During isothermal melting, away from the center of the spherulite, a cooperative melting of crosshatched lamellae increases the long period of the remaining thicker, mostly radial, lamellae in both ZN and M samples. As a consequence, the main long period increases as seen in Figure 9a. In the center of the spherulite crosshatching is very limited, and long-range lamellar periodicity during isothermal melting may depend on the arrangement of the primary dominant lamellae in this area. It remains constant in ZN iPP and decreases in the M sample as shown in Figure 9b.

It is possible to obtain information about the crystallite thickness, determined from the analysis of the one-dimensional correlation function.[32] Figure 10 gives a plot of the lamellar thicknesses, l_c, for both ZN-n and M-n polymers. Only the major scattering peak is resolved. Hence, what we observe is the evolution of the average lamellar thickness during the rapid heating, where crosshatched lamellae melt, and the subsequent evolution of the lamellar thickness during the period of isothermal melting. As shown in the figure, qualitatively the behavior between the ZN and M samples is similar during the rapid heating period. In this stage a high content of thinner crosshatched lamellae melt. The remaining lamellae then have a greater average thickness. The difference in the initial lamellar thickness

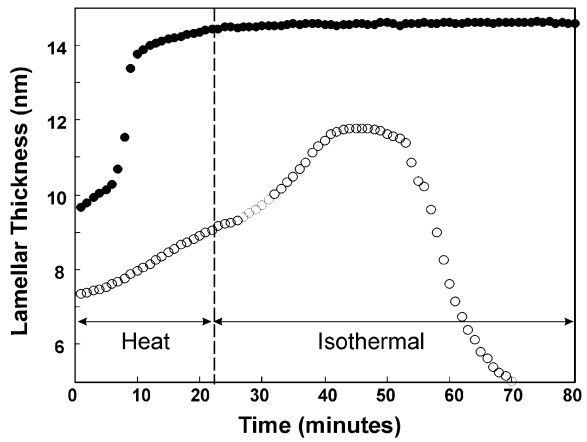

Figure 10. Lamellar thickness, l_c, determined from the one-dimensional electron density correlation function vs time. Ziegler−Natta iPP sample ZN-n, solid circles; metallocene iPP sample M-n, open circles. Times correspond to the treatments described in the caption of Figure 3.

between ZN-n (9.7 nm) and M (7.3 nm) is accentuated at the beginning of the isothermal stage (9 and 14.5 nm, respectively) due to the different content of crystallites that have melted from each poly(propylene) at this point. A much higher fraction of crystallites have melted in the ZN than in the M polymer as shown by the WAXS and invariant data of Figures 3 and 7.

The difference in the initial lamellar thickness between the ZN and M samples is consistent with the differences in the distribution of defects in both poly(propylenes). As demonstrated in recent works, the ZN poly(propylene) contains a small fraction of very long molecules with very high isotacticity, and the distribution of defects in all the molecules deviates from the random behavior.[33] The highly isotactic molecules lead to a fraction of much thicker lamellae in the ZN type sample. We speculate that the majority of these are the lamellae left at the early stages of the isothermal region in the ZN polymer. The fact that the thickness remains invariant during the first 80 min of the isothermal period is consistent with the notion that most crosshatched lamellae have melted, and only the thick, possibly radial, lamellae persist with a minor number of epitaxial sites. The small variation of the long spacing (Figure 9a) at the beginning of the isothermal stage and constancy in the rest of the period is in agreement with this structural scheme. With time (>80 min) enough nuclei melt leading to a decrease of the lamellae thickness and to complete melting (these data are not shown in Figure 10).

The metallocene sample lacks a fraction of almost defect free molecules, and then it lacks the fraction of very thick lamellae present in the ZN polymer. Therefore, the evolution of the lamellar thickness of this sample during the isothermal period (open symbols in Figure 10) is different than in the ZN sample. The lamellar thickness continues to increase up to about 12 nm and decreases sharply during the last 20 min up to complete melting. It is apparent that thinner crosshatched lamellae continue to melt during the early part of the isothermal region where the lamellar thickness is seen to increase. When most transverse lamellae are molten, the thickness of thicker radial lamellae remains constant and then decreases rapidly during progressive, possibly surface, melting.

On the basis of Babinet's principle of reciprocity,[31,35] there is an ambiguity in the assignment of the thickness determined from the correlation function. This length (found from the intersection of the extrapolation of the linear region at low z to the assumed baseline at the first minimum[32]) cannot be attributed unambiguously to the crystalline phase. Additional information is usually needed to confirm any assignment that is made.[35] In the present case, the decrease in l_c with time, as is illustrated in Figure 10, provides the necessary confirmation. The decease in l_c, in the latter part of the isothermal holding period, can be attributed to fusion, with the melting starting at the lamellar surfaces and proceeding inward. The ZN sample behaves in a similar manner when a longer time range is investigated. Melting would have an opposite effect on the thickness of the amorphous layer. In this manner the assignment of l_c is substantiated.

Conclusions

Real-time in-situ WAXS and SAXS studies confirm that isothermal melting kinetics takes place in isotactic poly(propylenes) in a temperature region between melting of transverse and dominant (radial) lamellae, i.e., when most transverse lamellae are molten. Thus, the results from X-ray scattering give substantial support to similar conclusions reached solely on studies involving differential scanning calorimetry. Melting kinetics is, apparently, unique to poly(propylene) as a consequence of a favorable nearly orthogonal epitaxial crystallization. What is observed is the instability of the dominant thicker lamellae due to the removal of the epitaxy. Both Ziegler−Natta and metallocene catalyzed polymers show this behavior. Hence, melting kinetics is a general phenomenon in poly(propylenes) that crystallize preferentially in the alpha or monoclinic modification at relatively low undercooling (T_c > ∼140 °C) when the crystallites are not subject to reorganization. Melting kinetics may be one of the reasons for the divergence in the reported equilibrium melting temperature of this polymer.[18−21]

The kinetics of the isothermal melting process of poly(propylenes) are affected by the initial lamellar morphology, which differs between a ZN-iPP and a metallocene type (as seen by AFM) due to a major difference in distribution of defects inter- and intramolecularly.[33,34] After crystallization at the same temperature, the melting kinetics of the metallocene iPP is significantly faster than those from the Ziegler type. ZN iPP contains a fraction of highly isotactic molecules that develop thicker lamellae and melt at significantly longer times than the crystallites from the metallocene iPP. The metallocene polymer did not show as clear crosshatching as the ZN iPP; the lamellae in the M iPP spherulites, of a segmented character, appear to be uniformly distributed. Thus, isothermal melting in M iPP is continuous and faster than for the ZN polymer. Despite the differences in magnitude and rate of isothermal melting, the process presents the same sigmoidal characteristics in both iPPs. Melting nuclei are presumably formed in dominant lamellae due to the disappearance of transverse ones in a first slow induction period. This is followed by a second stage of rapid cooperative melting of the dominant, radial lamellae. In a final stage the few remaining thickest lamellae melt slowly. Differences in defect microstructure of both types of iPPs lead to structural differences in lamellar perfection and

in the amount and nature of the transverse and radial lamellae. These differences provide a possible basis for the observed variation in melting kinetics between the ZN and M polymers.

Acknowledgment. U.S. Army Research Office Grant DAAH04-96-1-0009 and National Science Foundation Grant DMR-0094485 supported this work. The assistance of W. Huang and S. N. Magonov with the AFM images is also acknowledged.

References and Notes

(1) Padden, F. J., Jr.; Keith, H. D. *J. Appl. Phys.* **1966**, *37*, 4013.
(2) Binsbergen, F. L.; De Lange, B. G. M. *Polymer* **1968**, *9*, 23.
(3) Lotz, B.; Wittmann, J. C.; Lovinger, A. *J. Polym. Sci., Polym. Phys. Ed.* **1996**, *37*, 4979.
(4) Khoury, F. *J. Res. Natl. Bur. Stand., Sect. A* **1966**, *70*, 29.
(5) Padden, F. J.; Keith, H. D. *J. Appl. Phys.* **1973**, *44*, 1217.
(6) Lotz, B.; Wittmann, J. C. *J. Polym. Sci., Polym., Phys. Ed.* **1986**, *24*, 1541.
(7) Chi, C. MS Dissertation, Florida State University, 1997.
(8) Janimak, J. J.; Cheng, S. Z. D.; Giusti, P. A.; Hsieh, E. T. *Macromolecules* **1991**, *24*, 2253.
(9) Alamo, R. G.; Brown, G. M.; Mandelkern, L.; Lehtinen, A.; Paukkeri, R. *Polymer* **1999**, *40*, 3933.
(10) Norton, D. R.; Keller, A. *Polymer* **1985**, *26*, 704.
(11) Olley, R. H.; Bassett, D. C. *Polymer* **1989**, *30*, 399.
(12) Varga, J. *J. Mater. Sci.* **1992**, *27*, 2557.
(13) White, H. M.; Bassett, D. C. *Polymer* **1997**, *38*, 5515.
(14) When crystallization is carried out at high or relatively high undercoolings, superimposed on the thermogram is the manifestation of partial melting and recrystallization.[9,15]
(15) Ijima, M.; Strobl, G. *Macromolecules* **2000**, *33*, 5204.
(16) Huang, T. W.; Alamo, R. G.; Mandelkern, L. *Macromolecules* **1999**, *32*, 6374.
(17) Mandelkern, L.; Alamo, R. G. In *American Institute of Physics Handbook of Polymer Properties*; Mark, J. E., Ed.; AIP Press: New York, 1994.
(18) Phillips, R. A.; Wolkowicz, M. D. In *Polypropylene Handbook*; Moore, E. P. J., Ed.; Hanser: Munich, 1996.
(19) Lucas, J. C.; Alamo, R. G.; Mandelkern, L. *Polym. Chem. Div. Prepr.* **1994**, *35*, 408.
(20) Xu, J.; Srinivas, S.; Marand, H.; Agarwal, P. *Macromolecules* **1998**, *31*, 230.
(21) Mezghani, K.; Phillips, P. J. *Macromolecules* **1994**, *27*, 997.
(22) Westerman, L.; Clark, J. C. *J. Polym. Sci., Polym. Phys. Ed.* **1973**, *11*, 559.
(23) Zambelli, A.; Zetta, L.; Sacchi, C.; Wolfsgruber, C. *Macromolecules* **1972**, *5*, 440.
(24) Mizuno, A.; Tsutsui, T.; Kashiwa, N. *Polymer* **1992**, *33*, 254.
(25) Grassi, A.; Zambelli, A.; Resconi, L.; Albizzati, E.; Mazzocchi, R. *Macromolecules* **1988**, *21*, 617.
(26) Busico, V.; Cipullo, R.; Monaco, G.; Vacatello, M.; Segre, A. L. *Macromolecules* **1997**, *30*, 6251.
(27) Isasi, J.; Mandelkern, L.; Galante, M. J.; Alamo, R. G. *J. Polym. Sci., Polym. Phys. Ed.* **1999**, *37*, 323.
(28) Dai, P.; Cebe, P.; Capel, M. *J. Polym. Sci., Polym. Phys. Ed.* **2002**, *40*, 1644.
(29) Dai, P.; Cebe, P.; Capel, M.; Alamo, R.; Madelkern, L. *J. Appl. Crystallogr.* **2000**, *33*, 714.
(30) Bark, M.; Zachmann, H. G.; Alamo, R.; Mandelkern, L. *Makromol. Chem.* **1992**, *193*, 2363.
(31) Balta-Calleja, F. J.; Vonk, C. G. *X-ray Scattering of Synthetic Polymers;* Jenkins, A. D., Ed.; Elsevier: Amsterdam, 1989.
(32) Strobl, G. R.; Schneider, M. *J. Polym. Sci., Polym. Phys. Ed.* **1980**, *18*, 1343.
(33) Alamo, R. G.; Blanco, J. A.; Agarwal, P.; Randall, J. C. *Macromolecules* **2003**, *36*, 1559.
(34) Randall, J. C.; Alamo, R. G.; Agarwal, P.; Ruff, C. *Macromolecules* **2003**, *36*, 1572.
(35) Jonas, A. M.; Russell, T. P.; Yoon, D. Y. *Macromolecules* **1995**, *28*, 8491.

MA025987Z